Radiative ablation to low-*Z* matter

Jiamin Yang,[1,*] Jiatian Sheng,[2] Yaonan Ding,[1] Yunsheng Li,[2] Shaoen Jiang,[1] Tinggui Feng,[2] Zhijian Zheng,[1] Kexu Sun,[1] Wenghai Zhang,[1] Yanli Cui,[1] and Jiushen Cheng[1]

[1]*National Key Laboratory of Laser Fusion, Research Center of Laser Fusion, P.O. Box 919-986, Mianyang 621900, People's Republic of China*

[2]*Institute of Applied Physics and Computational Mathematics, Beijing 100088, People's Republic of China*

(Received 3 May 2002; published 30 September 2002)

Eight beams of 0.35-μm laser with pulse duration of about 1.0 ns and energy of 260 J per beam were injected into a cylindrical cavity to generate intense x-ray radiation on the Shengguang II high power laser facility. Plastic foils with a thickness in the range of about 3.0–45 μm were attached on the diagnostic hole of the cavity and ablated by the intense x-ray radiation. The radiative energy transport through plastic foils with different thicknesses has been studied experimentally. The burn-through time of the plastic foils has been obtained. For comparison, we also simulated the experimental results with Planckian and non-Planckian x-ray spectrum source, respectively. It is shown that for thick plastic foil the simulation with non-Planckian x-ray spectrum source is in good agreement with the experiment.

DOI: 10.1103/PhysRevE.66.036410 PACS number(s): 52.50.Jm, 44.40.+a, 47.70.Mc

I. INTRODUCTION

In the scheme of indirectly driven inertial confinement fusion (ICF), the driven x-ray radiation is first generated in a cavity of high-*Z* matter. Then the intense radiation ablates the low-*Z* wall of a DT pellet, leading to its compression and to thermonuclear burn. As the radiation that drives the implosion of the fuel capsule also ablates the interior walls of a high-*Z* cavity to form radiation heat wave, the propagation of the radiation heat wave into the interior walls of the cavity loses some partition of radiation energy and changes the coupling efficiency of radiation energy to the fuel capsule. The radiation heat waves [1–6] in the high-*Z* matter have been observed theoretically and experimentally. In order to obtain the highest hydrodynamic efficiency in the radiation-driven implosion of the capsule, it is also crucial to know the radiative energy transport and the propagating speed of the heating wave in the low-*Z* shell of the capsule. Therefore, a series of investigations on reemission and the propagation of the heating wave for low-*Z* matter have been carried out [7–19]. In most experiments published previously, relatively thin low-*Z* foils (thinner than 5 μm) were used due to the lower incident x-ray radiation source and the x-ray source spectrum was assumed to be Planckian. It was indicated [15] that the gold *O*-, *N*-, and *M*-band emissions in the x-ray source have no obvious effects on the simulations of the experiments. With the completion of upgraded Shengguang II high power laser facility in China, the intense x-ray radiation source was obtained by injecting eight laser beams into cylindrical cavity from its two ends. The intense radiation was applied to ablate the low-*Z* matter with thickness of up to 45 μm. It is found that there exist intense gold *O*-, *N*-, and *M*-band emissions in our x-ray source, and these band emissions should be taken into account in the simulation of radiation ablation to thicker low-*Z* matter.

II. EXPERIMENTAL ARRANGEMENT

The experiments were carried out with up to eight beams of 0.35-μm laser on the Shengguang II laser facility in Shanghai. The scheme of the experiments is shown schematically in Fig. 1. Two bundles of four laser beams enter the cylindrical cavity from its two ends to generate intense x-ray radiation. The laser energy per beam is about 260 J with flat-top pulse duration of about 1.0 ns. The diameter of the cylindrical cavity is 800 μm and its length 1400 μm. Two circular diagnostic holes with diameter of 280 and 300 μm were opened about the midplane. The diagnostic hole with diameter of 300 μm was left open or covered by a single layer of plastic foil with different thicknesses in different experimental shots, as shown in Fig. 1. The x-ray radiation signals from the radiation source (when the hole was left open) or the rear of the plastic foil were measured with a soft x-ray spectrometer (SXS). The soft-x-ray spectrometer has seven energy channels that covers the x-ray energy range of about 50–1500 eV. The grazing incident mirrors are used in the spectrometer to cut off higher energy x rays. As the soft-x-ray spectrometer has a fiducial signal, the delay of x-ray signals at seven energy channels from the rear of different thickness plastic foil can be obtained by varying the thickness of plastic foil in different shots. In the measurement the laser parameters and the targets except for the sample attached on the hole were kept the same. The intense x-ray radiation that ablates the low-*Z* material was monitored by another soft-x-ray spectrometer from the 280-μm circular diagnostic hole. A $2000l/mm$ transmission grating spectrometer was also used to measure the time-integrated x-ray spectrum from the laser-injected hole in the direction of 30° with respect to the axes of the cylindrical cavity. In the experiments, the plastic foils with thicknesses of 3.18, 4.17, 7.83, 15.0, and 45.0 μm were used as test sample. The density of the plastic foil is about 1.0 g/cm^3.

*Present address: Research Center of Laser Fusion, CAEP, P.O. Box 919-986, Mianyang 621900, People's Republic of China. FAX: 0816-2484270.

Email address: yjm70018@my-public.sc.cninfo.net

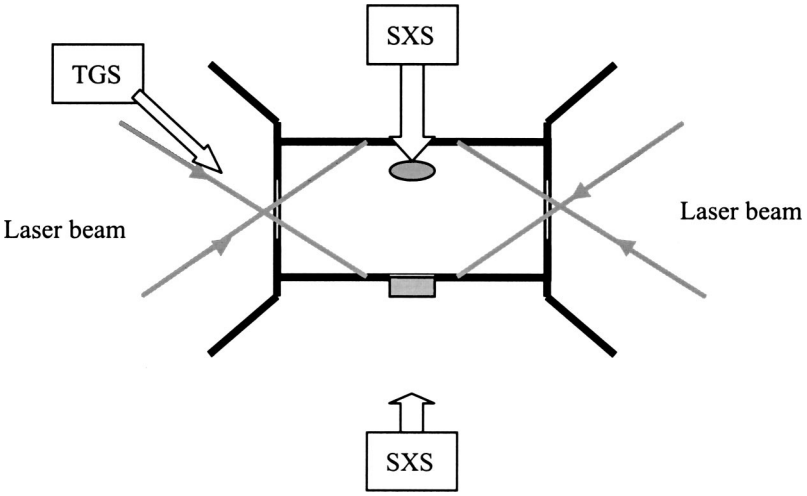

FIG. 1. The schematic view of the experimental setup. SXS: soft-x-ray spectrometer. TGS: transmission grating spectrometer.

III. EXPERIMENTAL RESULTS AND DISCUSSIONS

The time-dependent hohlraum equivalent radiation temperature was shown in Fig. 2. The temperature rises relatively fast at first, reaching about 130 eV, then increases slowly to the maximum temperature of 143 eV. The time-integrated x-ray source spectrum measured with the transmission grating spectrometer was shown in Fig. 3. The *O*-, *N*-, and *M*-band emissions of the gold plasma were seen obviously.

The time-dependent equivalent radiation temperature measured from the rear of the plastic foils with the soft-x-ray spectrometer was illuminated in Fig. 4. It can be seen that the maximum radiation temperature decreases as the thickness of the plastic foil increases, and the time delay of the temperature increases as the thickness of the plastic foil does except for the 45-μm-thick plastic foil.

The typical time-integrated x-ray spectrum measured with the transmission grating spectrometer from the rear of the 15.0-μm-thick CH sample was shown in Fig. 5. The obvious carbon *K* absorption edge has been seen.

The x-ray signals at photon energy of about 300 to 450 eV (correspond to Ti channel of the soft-x-ray spectrometer) were shown in Fig. 6. The delay of the x-ray signals from the radiation-ablated low-*Z* sample relative to the driving radiation was seen clearly. The delay increases as the thickness of the plastic foil does. For radiation ablation to low-*Z* plastic foil, the radiation absorbed by low-*Z* matter results in increased temperature and ionization of the plastic layer. The temperature rise shifts the *K* absorption edge of carbon ~278 eV to the higher energy of about 400–500 eV, as shown in Fig. 7, in which the opacity of carbon at temperature of 30 and 100 eV has been calculated using an unresolved transition array (UTA) model [22,23]. The opacity of the ionized plastic layer behind the ablation surface decreases sharply in the x-ray energy range of 278–400 eV ~500 eV. When burn through of the radiation-ablated plastic foil occurs the x-ray signal in the energy range of 278–400 eV ~500 eV will increase immediately. Therefore, we define the breakout time of the heating wave as the time at which the radiation at about 300–450 eV from the rear of the low-*Z* sample reaches 50% of its peak. Similarly, the beginning time of radiation ablation is defined as the time at which the x-ray source signal (the diagnostic hole left open) reaches 10% of its maximum intensity. In this experiment, the burn-through time of the low-*Z* sample as a function of its thickness was obtained, as illustrated in Fig. 8. It is also clearly seen that the burn-through time of the plastic foil is approximately linearly proportional to its thickness. Therefore, the propagating velocity of the radiation heat wave in the plastic foil is constant in this experiment, and the mass ablation rate of about 1.48×10^6 g/cm^2 s is obtained by fitting linearly the experimental data, shown in Fig. 6. Substituting the measured peak radiation temperature of about 140 eV, as shown in Fig. 2, into the Eq. (52) of the Ref. [24], the mass ablation rate of about 8.23×10^5 g/cm^2 s is obtained and is smaller than the measured one by 45%. The reason may be that the intense *M*-band emission in our x-ray source as shown in Fig. 3 could be transported into the CH sample more deeper and could preheat the CH sample.

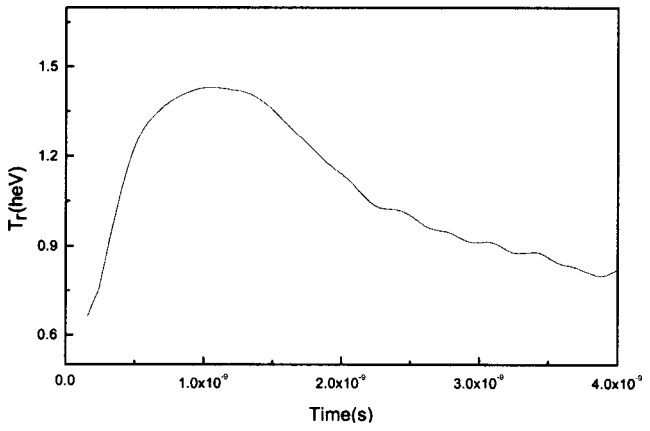

FIG. 2. The radiation temperature of the cylindrical cavity versus time measured with an absolutely calibrated multichannel soft-x-ray spectrometer from the circular diagnostic hole with diameter of 280 μm.

For a detailed analysis, the experiments were also simulated using a one-dimensional (1D) multigroup radiation transport code RDMG [20,21]. The x-ray source radiation in the simulations was assumed to be a Planckian or non-Planckian spectrum with the measured equivalent radiation temperature, as shown in Fig. 2, and divided into 100 groups

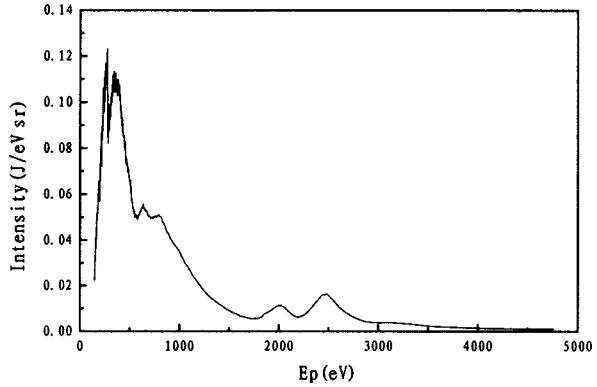

FIG. 3. Time-integrated x-ray spectrum from the laser-injected hole of the cylindrical cavity, measured with transmission grating spectrometer.

in the energy range of 50–5000 eV. In the case of non-Planckian spectrum, the x-ray spectrum measured with the transmission grating spectrometer, as shown in Fig. 3, is used as incident x-ray source spectrum in the simulation. The incident radiation flux is also assumed to be isotropic. Ions and electrons except for radiation in the plasma are thought to reach equilibrium, respectively. But the assumption of complete thermodynamic equilibrium between radiation and matter is not required. Simulations of radiative ablation to the plastic foil, which were used in the experiment, were carried out.

Figure 9 presents the simulated radiation temperatures as a function of time from the rear of plastic foils with different thicknesses in both cases of Planckian and non-Planckian spectrum sources. For 3.18- and 7.83-μm-thick CH plastic foils, the simulated radiation temperatures in both cases are similar and in good agreement with the measured ones. For 15.0- and 45.0-μm-thick CH plastic foils, the simulated radiation temperatures using non-Planckian spectrum source are also consistent with the measured ones. But the simulated temperatures using Planckian spectrum source are apparently lower than the measured ones.

Figure 10 gives the simulated spectral intensity versus time at four x-ray energies, i.e., 392, 542, 914, and 174 eV,

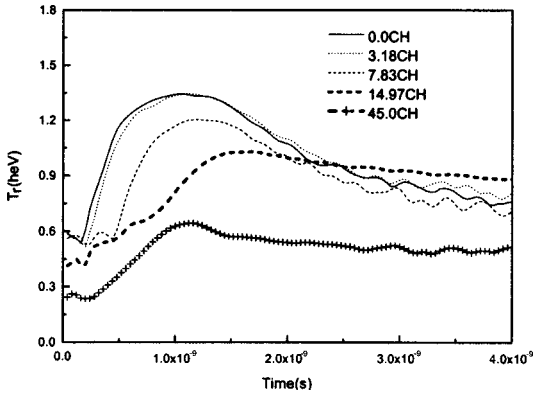

FIG. 4. The radiation temperature versus time from the rear of the radiation-ablated plastic foils with different thickness, measured with the soft-x-ray spectrometer.

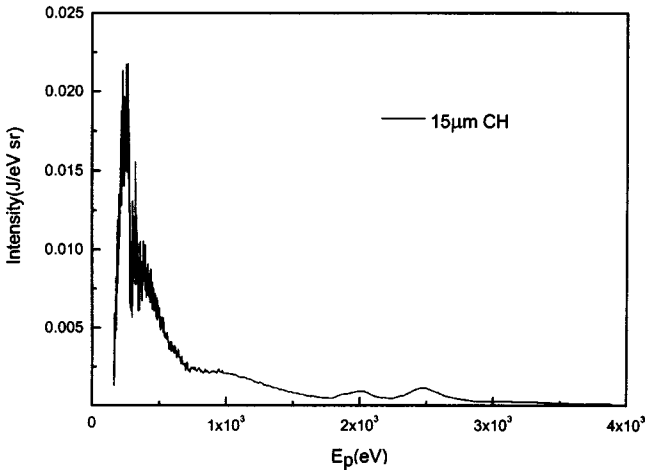

FIG. 5. The time-integrated x-ray spectrum from the rear of the 15.0-μm-thick CH sample, measured with a transmission grating spectrometer.

from the rear of the plastic foils in the case of non-Planckian spectrum source. The spectral intensities at 392 and 542 eV from the rear of the plastic foil are delayed obviously compared with the spectral intensities at 914 and 174 eV. The reason is that the opacity of the cold plastic foil at higher energy of 914 and 1741 eV is much lower than that at 392 and 542 eV. When the driving radiation is incident on the plastic foil, the x ray at the higher energies shines through the foil immediately, but the x rays at 392 and 542 eV cannot pass through the plastic foil until burn through of the plastic foil occurs.

The calculated burn-through time of the test sample was obtained from the simulations, with the same definitions of breakout time and beginning time of driving radiation as those in the above experimental results. Comparison of the theoretical burn-through time with the experimental ones was shown in Fig. 11. There exists little difference for the calculated burn-through time of the 3.18-, 4.17, and 7.83-μm-thick plastic foils in both cases. But for 15-μm-thick plastic foil, the simulated burn-through time using Planckian spectrum source is much larger than that using non-Planckian spectrum source. For simulation using non-

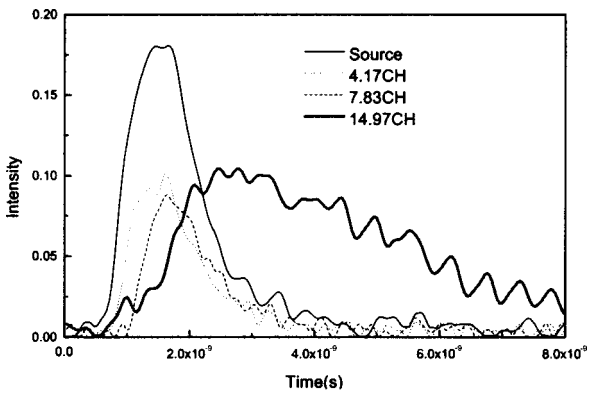

FIG. 6. The x-ray signals at photon energy of about 300–450 eV vs time from the rear of the plastic foils with different thickness, measured with SXS.

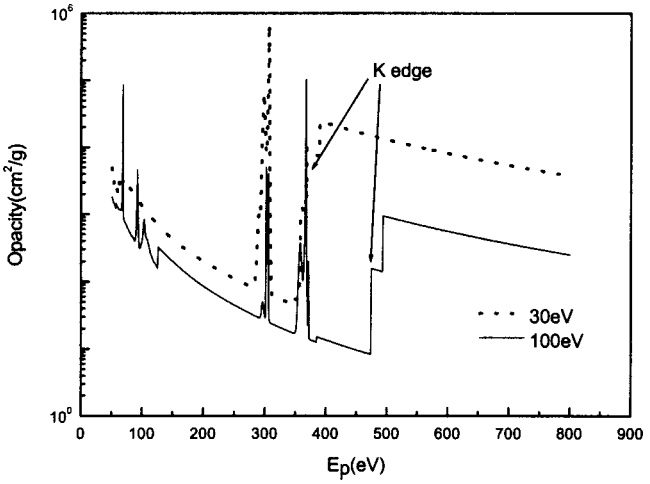

FIG. 7. The calculated opacity of carbon at temperature of 30 and 100 eV, the density of carbon was assumed to be 0.01 g/cm^{-3}.

Planckian spectrum source the calculated burn-through time is also approximately linearly proportional to the CH thickness, which is similar as the experiment, and the estimated theoretical mass ablation rate of the plastic foil is about 1.85×10^{6} g/cm^{2} s by fitting the calculated data linearly. This result is only larger than the experimental one by 25%. But for simulation using Planckian spectrum source no linear relation between the burn-through time and CH thickness exist for plastic foils with thickness of 3.18–15.0 μm. There also exit a deviation that the simulated absolute burn-through times in both cases are larger than the measured ones. The deviation may come from the following aspects.

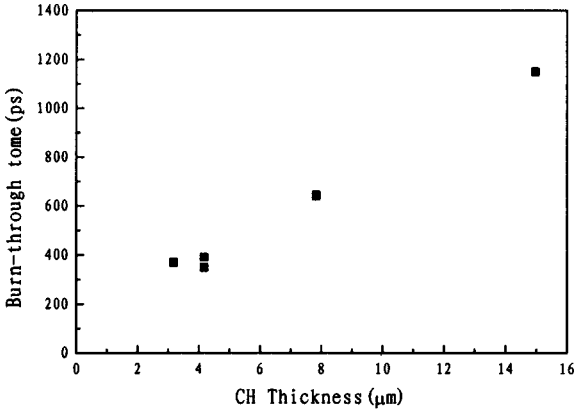

FIG. 8. The experimental results of the burn-through time vs its thickness for the plastic foils.

(1) The measured x-ray source signal that was used to determine the beginning time of the driving radiation is the reemission radiation of the gold walls. However, the reemission radiation is time delayed with respect to the real driving radiation. Therefore, the measured burn-through time is smaller than the real one.

(2) The measured radiation temperature of the driving source, which was used as x-ray source in the simulations is also the reemission radiation temperature of the inner walls. Since the reemission efficiency of the inner walls is lower than 1, especially during the beginning time of the driving source, the driving radiation in the simulations is less intensive than the real one during the beginning time, which may results in larger burn-through time in the simulation.

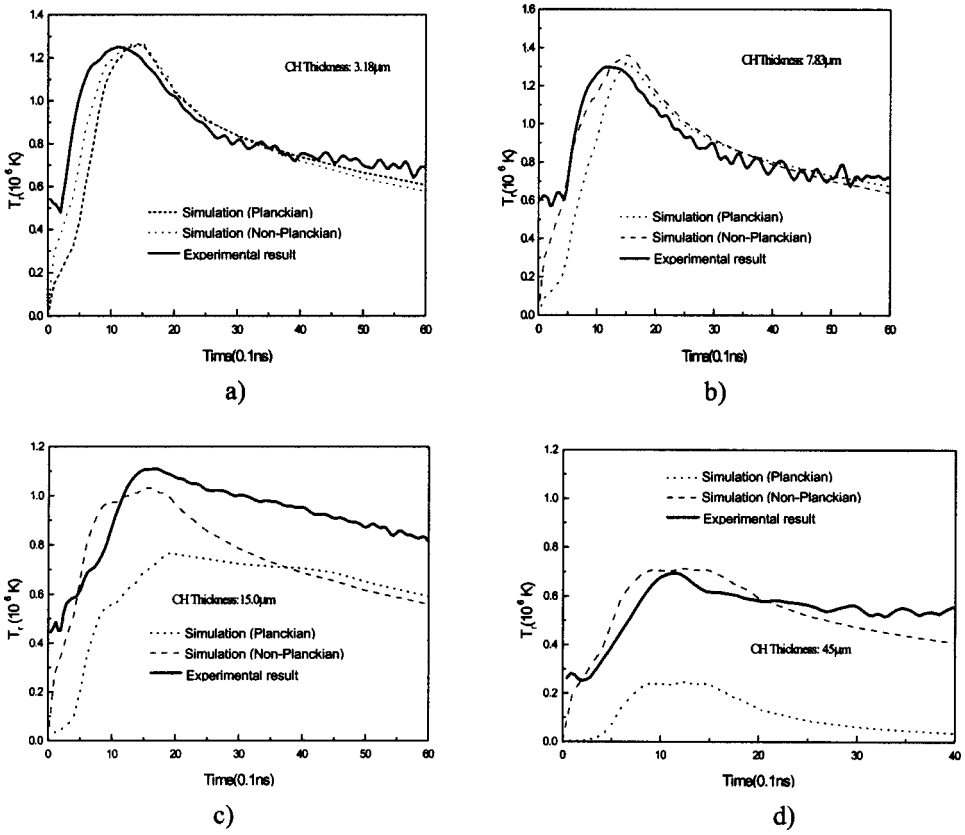

FIG. 9. Comparison of the simulated time-dependent radiation temperatures from the rear of plastic foils with different thicknesses with the experimental results. (a) CH thickness: 3.18 μm, (b) CH thickness: 7.83 μm, (c) CH thickness: 15 μm, and (d) CH thickness: 45 μm.

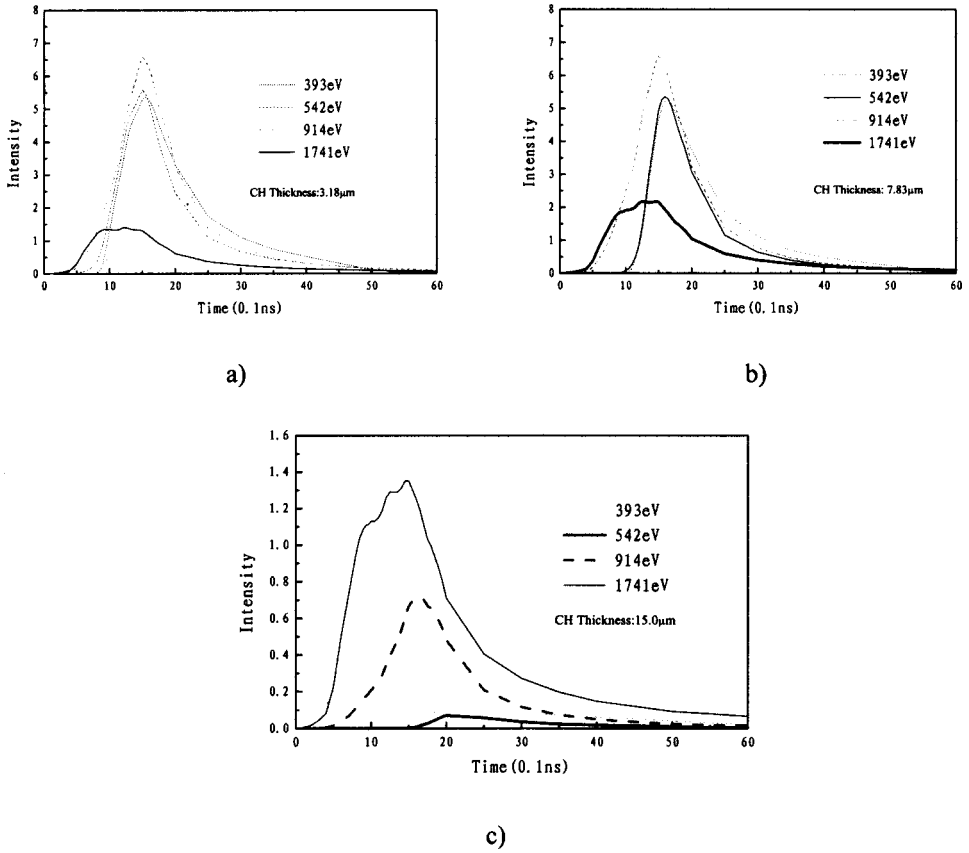

FIG. 10. The simulated time-dependent x-ray signals at four photon energies from the rear of the radiation-ablated plastic foils, using the RDMG code. (a) CH thickness: 3.18 μm, (b) CH thickness: 7.83 μm, and (c) CH thickness: 15 μm.

(3) Other reasons, for example, higher opacity was used in the simulation. However, further investigations need to be carried out to definitely explain the derivations.

IV. CONCLUSIONS

Intense x-ray radiation source with peak temperature up to 143 eV was generated on the newly upgraded Shengguang II laser facility. It is shown by the measurements that this radiation source has intense gold *O*-, *N*-, and *M*-band emissions. Using this intense x-ray radiation source, the radiative ablation to low-*Z* plastic foils has been experimentally studied. The experimental results show that the maximum radiation temperature from the rear of the plastic foils decreases as the thickness of the plastic foil increases. The time delay of the temperature increases as the thickness of the plastic foil does except for the 45-μm-thick plastic foil. The burn-through time of the plastic foil is approximately linearly proportional to its thickness, and the mass ablation rate of the plastic foil is about 1.48×10^{6} g/cm^2 s. For an analysis of the experimental results, a one-dimensional multigroup radiation transport code RDMG was used to simulate the experiments. In the simulations two types of x-ray spectra, i.e., Planckian and non-Planckian spectrum (with and without the inclusion of the gold *O*-, *N*-, and *M*-band emissions), were used as incident x-ray source spectrum. It is shown, by comparison of the simulations with the experiments, that for thinner plastic foils the simulations in both cases of Planckian and non-Planckian source spectrum generate nearly the same results, as indicated by Edwards, Barrow, and Willi [15]. But for thicker plastic foils, such as 15-μm-thick plastic foil in this experiment, significant influence of the gold *O*-, *N*-, and *M*-band emissions on the overall predicted results were seen in the simulations. Moreover, the simulation with the inclusion of the gold *O*-, *N*-, and *M*-band emissions in the x-ray source spectrum can reproduce the experiments in general.

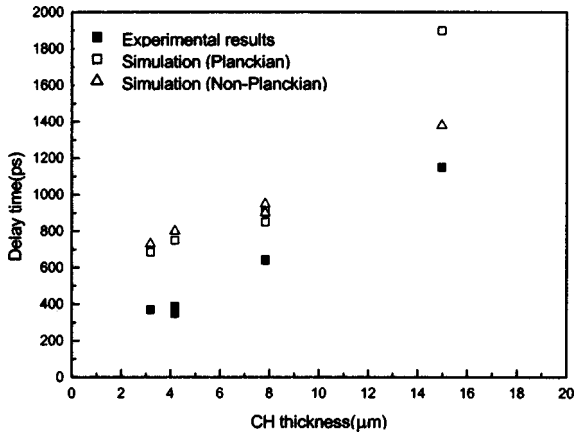

FIG. 11. Comparison of the simulated burn-through times in both cases (Planckian and non-Planckian spectrum source) for the plastic foils with the experimental ones.

ACKNOWLEDGMENTS

This work was supported by National High-Tech 863-804 program in China. The authors also would like to thank the operation staffs of the Shengguang II laser facility for their cooperation.

[1] R. E. Marshak, Phys. Fluids **1**, 24 (1958).
[2] R. Sigel *et al.*, Phys. Rev. Lett. **65**, 587 (1990).
[3] R. Sigel *et al.*, Phys. Rev. A **45**, 3987 (1992).
[4] J. L. Porter *et al.*, UCRL Report No. LR-105821-94-4 (unpublished), p. 125.
[5] T. J. Orzechowski *et al.*, Phys. Rev. Lett. **77**, 3545 (1996).
[6] R. Pakula and R. Sigel, Phys. Fluids **28**, 232 (1985).
[7] K. Nishihara, Jpn. J. Appl. Phys., Part 2 **2**, L571 (1982).
[8] T. Yabe *et al.*, Jpn. J. Appl. Phys., Part 2 **22**, L88 (1983).
[9] N. Kaiser, J. Meyer-ter-Vehn, and R. Sigel, Phys. Fluids B **1**, 1747 (1989).
[10] T. Endo, H. Shiraga, and Y. Kato, Phys. Rev. A **42**, 918 (1990).
[11] N. W. Kaiser, J. Meyer-ter-Vehn, and R. Ramis, Laser Part. Beams **9**, 759 (1991).
[12] A. R. Piriz and F. G. Tomasel, Phys. Rev. A **45**, 8787 (1992).
[13] T. Mochizuki *et al.*, Phys. Rev. A **36**, 3279 (1987).
[14] T. Endo *et al.*, Phys. Rev. Lett. **60**, 1022 (1988).
[15] J. Edwards *et al.*, Europhys. Lett. **11**, 631 (1990).
[16] J. Edwards *et al.*, Phys. Rev. Lett. **67**, 3780 (1991).
[17] T. Afshar-rad *et al.*, Phys. Rev. Lett. **73**, 74 (1994).
[18] I. B. Foldes, K. Eidmann, and Th. Lower, Phys. Rev. E **50**, 690 (1994).
[19] I. B. Foldes and K. Eidmann, Laser Part. Beams **14**, 487 (1996).
[20] Xu Yan *et al.*, High Power Laser Part. Beams **13**, 329 (2001).
[21] Lai Dongxian *et al.*, High Power Laser Part. Beams **13**, 64 (2001).
[22] J. Yan, Y. Zh. Qu, and J. M. Li, High Power Laser Part. Beams **11**, 65 (1999).
[23] J. M. Yang *et al.*, Chin. Phys. Lett. **18**, 550 (2001).
[24] John Lindl, Phys. Plasmas **2**, 3933 (1995).